Three-dimensional optical polarization tomography of single molecules

Michael Prummer, Beate Sick, Bert Hecht,[a] and Urs P. Wild
Physical Chemistry Laboratory, Swiss Federal Institute of Technology, ETH-Zentrum, Universitätsstr. 22, CH-8092 Zürich, Switzerland

(Received 22 October 2002; accepted 5 March 2003)

We apply the concept of tomography to polarization-sensitive optical microscopy of single fluorophores to determine the three-dimensional orientation of molecular absorption dipoles with isotropic sensitivity. Wide-field microscopy provides the opportunity to monitor simultaneously three-dimensional rotation and two-dimensional translation of many molecules in parallel. For orientation determination the molecules are illuminated from different directions of incidence with linearly polarized light. In each exposure the excitation along a particular projection of the absorption dipole on the electric field leads to a distinct fluorescence intensity. Five exposures are sufficient to determine the full orientation of the fluorophores. To demonstrate the potential of the method we determine the orientation and position of individual immobilized lipid membrane markers. The shot-noise-limited isotropic angular resolution is 2°. For time-resolved studies the bandwidth can be expanded up to 200 Hz. © *2003 American Institute of Physics.*
[DOI: 10.1063/1.1569848]

I. INTRODUCTION

Experiments in which single chromophores serve as markers or local probes for their immediate environment nowadays are a standard tool to unravel dynamical processes on a molecular scale.[1,2] By definition, single-molecule experiments do not suffer from ensemble averaging and are therefore ideally suited to investigate structural heterogeneities in lipid membranes,[3,4] uncorrelated dynamics in motor proteins[5,6] or trans-membrane proteins,[7] and intermediates in elementary chemical[8,9] and folding reactions.[10,11] Another consequence of the absence of averaging in single-molecule experiments is the possibility to select individual molecules with desired properties out of an ensemble.[12] In fluorescence experiments, this selection can be performed in space, time, energy, and polarization.

Position, relative distance, and orientation of fluorophores attached to target molecules are the observables that report on the mechanistic aspects of steady state and dynamic behavior of macromolecules.[13] By exploiting single-pair fluorescence resonance energy transfer[14] (FRET) and polarization-sensitive fluorescence detection,[15,16] a ruler and a protractor on a molecular scale have been developed.

In both concepts, knowledge about the three-dimensional (3D) orientation of the chromophore's dipole moment[17–19] is important. For example, the transfer efficiency in FRET not only depends on the interdye distance but also on the mutual orientation of donor and acceptor. More precise distance measurements therefore become possible when the 3D orientation of both the donor emission dipole and the acceptor absorption dipole are known.[14] However, because of experimental constraints, usually only the orientation of the projection of the transition dipoles into the image plane can be determined.[15,16] Furthermore, the fluorescence lifetime and, as a consequence, the quantum yield of dye molecules close to an interface depend on the out-of-plane component of their dipole moments.[20] Also the detection efficiency depends on the emission dipole orientation. Therefore, without *a priori* knowledge, only ambiguous information can be obtained by only considering a 2D projection of the dipole moment.

Here we present a new method of single-molecule microscopy: i.e., three-dimensional optical polarization tomography (3D-OPTO). 3D-OPTO allows us to determine the three-dimensional orientation of many individual molecular absorbers in parallel with isotropic sensitivity. Wide-field fluorescence microscopy is used for parallel real-time imaging of single fluorophores close to an interface. The orientation determination is based on sequential excitation with appropriately polarized beams from two perpendicular directions of incidence. Five exposures are sufficient to sample the full orientational space occupied by the chromophores. Usually, absorption dipole moments can only be determined on a one-by-one basis using confocal microscopy.[21] Knowing the dipolar orientation, 3D-OPTO facilitates highly selective excitation of otherwise indistinguishable fluorophores. As an example, we determine the steady-state orientational distribution of immobilized dye molecules, widely used to label phospholipid membranes. Our method holds promise to monitor orientational as well as spatial diffusion of a large number of molecules in parallel down to a 100 ms time scale.

II. MATERIALS AND METHODS

A. Sample preparation

Samples containing isolated molecules were prepared by spin casting (9600 rpm) of 10 μl of a solution of poly-

[a]Author to whom correspondence should be addressed. Current address: Nano-Optics group, Institute of Physics, University of Basel, Klingelbergstr. 82, CH-4056 Basel, Switzerland. FAX: +41 61 267 3795. Electronic mail: bert.hecht@nano-optics.ch

 © 2003 American Institute of Physics

Downloaded 27 May 2003 to 128.178.16.148. Redistribution subject to AIP license or copyright, see http://ojps.aip.org/jcpo/jcpcr.jsp

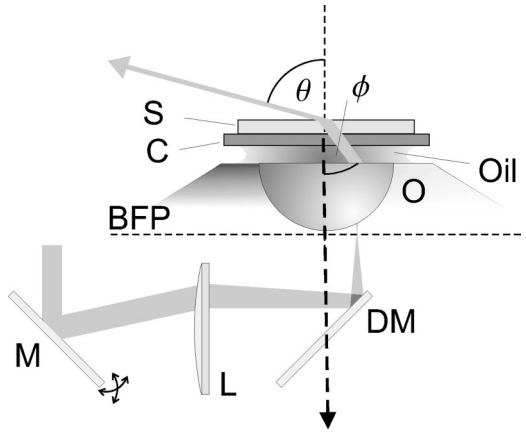

FIG. 1. Setup: a polarized laser beam is expanded and collimated to a diameter of 8 mm and directed onto a tiltable mirror (M) in the focal plane of the lens (L, 700 mm focal length). The lens focuses the beam into the back focal plane (BFP) of an oil immersion microscope objective (O) (Leica, 100×, NA 1.3) via a dichroic mirror (DM). The resulting collimated beam exits the objective, traverses the sample, and is refracted at the polymer–air interface. The sample consists of a cover slip (C) coated with a 30-nm PMMA film doped with the chromophore. ϕ: angle of incidence of the beam onto the polymer–air interface. θ: angle of the refracted light outside the sample. Fluorescence from the sample (dashed arrow) is directed onto a CCD camera.

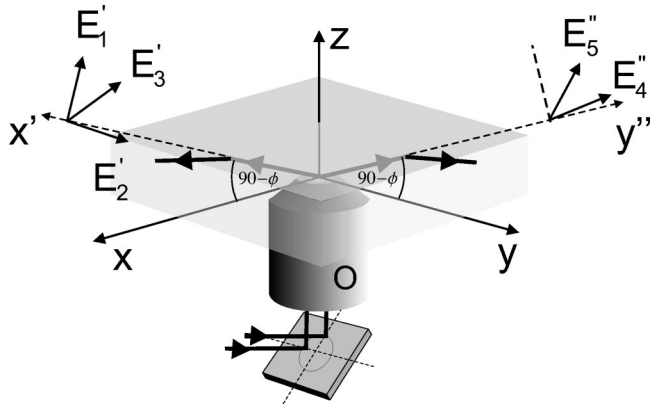

FIG. 2. Illumination geometry: first direction of incidence: (1) p polarization (E_1'), (2) s polarization (E_2'), and with (3) a polarization turned away from p polarization by 45° (E_3'). Second direction of incidence: (4) s polarization (E_4'') and with (5) polarization turned by 45° (E_5''). x, y, and z denote the axes of the laboratory frame of reference, x' and y'' indicate respective axes of the tilted frames. The beam can be directed by choosing the correct offset with respect to the optical axis of the objective (O).

methylmethacrylate (PMMA) in toluene (0.07% wt) containing 1 nM of the dye 1,1′-dioctadecyl-3,3,3′,3′-tetramethylindocarbocyanine (DiI) onto standard glass cover slips. Cover slips were cleaned by baking at 500 °C for 2 h. The refractive indices of PMMA is 1.48. Differences between the refractive index of PMMA and glass are negligible. Atomic force microscopy of the polymer films near a scratch revealed a smooth surface and a film thickness of about 30 nm.

B. Single-molecule wide-field microscopy

We used a Nd:YAG-laser frequency doubled to 532 nm at an intensity of approximately 1 kW/cm^2 to excite a large number of single molecules in parallel by illumination of a 30-μm-diam circular spot within the field of view of the microscope. The optical path is sketched in Fig. 1. The laser beam is expanded and collimated to a diameter of 8 mm. Its polarization is adjusted by means of a λ/2 plate. It is directed onto a tiltable mirror in the focal plane of a lens with 700 mm focal length. The lens focuses the beam into the back focal plane of an oil immersion microscope objective (O)(Leica, 100×, NA 1.3). This results in a collimated beam exiting the objective, traveling through the sample and being refracted at the polymer-air interface. Note that the optical path is adapted from objective-type total internal reflection fluorescence microscopy[22] (TIRFM). The angle of incidence ϕ of the beam onto the polymer–air interface can be adjusted by means of its offset to the optical axis in the back focal plane of the objective. Measurement of ϕ is accomplished by measuring the angle θ of the refracted light outside the sample as indicated in Fig. 1. We chose an angle of incidence ϕ at which the reflection coefficient for a p-polarized incoming beam vanishes: i.e., $\phi = 34.05°$. The corresponding angle θ is then 56°. Using this geometry the field at the position of a molecule inside the polymer film is very much simplified. We point out that the setup is also compatible with aqueous environment. In this case $\theta = 48°$ results in zero reflectivity for p-polarized light.

Single-molecule fluorescence is collected by the same objective that is used for excitation and imaged onto a detector. A Peltier-cooled slow scan charge coupled device (CCD) (PCO, Kehlheim, Germany) was used to record fluorescence images at a resolution of 300 nm and an integration time of 1 s (see Fig. 3). The use of intensified camera equipment or avalanche photo diodes (at the expense of parallel recording) can reduce the integration time per image to 1 ms. The time between images can be neglected because beam directions and polarizations can be switched very fast by, e.g., electro- or acusto-optical means. As compared to other techniques which require defocusing or aberrations to resolve orientation,[17–19] here the full signal-to-background ratio and the full diffraction-limited resolution can be exploited when imaging single molecules.

Our approach is to extract the Cartesian components of the absorption dipole from the variation of the fluorescence rate of a single molecule when illuminated by different excitation polarizations from different directions of incidence. Maximum sensitivity is provided by using two orthogonal planes of incidence, i.e., the $x-z$ and $y-z$ planes. The laboratory frame of reference is defined as sketched in Fig. 2. For the theoretical analysis we define two additional frames of reference that are tilted around the y axis and x axis by an angle of $90° - \phi$. The quantities in the two tilted coordinate systems are denoted by a prime and double prime, respectively. For the first direction of incidence, the beam in the glass (polymer) travels towards positive values along the x' axis. Three CCD images are recorded with (1) p polarization (E_1'), (2) s polarization (E_2'), and (3) a polarization turned away from p polarization by 45° (E_3') (see Fig. 2). For the second direction of incidence, the beam travels towards positive values along the y'' axis. Two additional CCD images

Downloaded 27 May 2003 to 128.178.16.148. Redistribution subject to AIP license or copyright, see http://ojps.aip.org/jcpo/jcpcr.jsp

are recorded with (4) *s* polarization (E_4'') and with (5) a polarization turned by 45° (E_5'') (see Fig. 2).

C. Theory and data analysis

The fluorescence count rate of a fluorophore far from saturation is given by

$$R = c|\hat{\mathbf{d}}\cdot\vec{\mathbf{E}}(\vec{\mathbf{r}})|^2, \tag{1}$$

where c is a constant including the detection efficiency and the absorption cross section, $\hat{\mathbf{d}}$ is the unit vector along the absorption dipole moment of the molecule, and $\vec{\mathbf{E}}(\vec{\mathbf{r}})$ is the electric field vector of the excitation beam at the position of the molecule.

In earlier experiments it has been shown that the 2D projection of a dipole in the plane perpendicular to the direction of incidence can be obtained with high precision by recording the fluorescence rate as function of the polarization direction $R = R_0 \cos^2(\alpha)$, where α is the angle between the direction of polarization and the dipole projection and R_0 is a constant.[16] Subsequent fitting can be used to determine α up to an integer multiple of π. However, it is possible without the need of fitting the $\cos^2(\alpha)$ characteristics to determine the 2D projection of the dipole moment from a minimum of three data points with sufficient accuracy. The benefit of this reduction of data points is a dramatic increase of the time resolution. Generalization of our concept to three dimensions requires the direction of incidence to be changed and two additional data points to be recorded.

From the first two exposures in the first direction of incidence, the modulus of the dipole components in the $y'-z'$ plane of the system can be determined from Eq. (1) as

$$d_z' = \pm(R_1/E_1'^2)^{1/2}, \tag{2}$$

$$d_y' = \pm[R_2/(1.34^2 E_2'^2)]^{1/2}. \tag{3}$$

Here (and in the following) R_i is the peak-integrated fluorescence count rate of any single-molecule peak in exposure i and E_i' is the incident electric field (including the constant c) at the position of the molecule in exposure i. It is important to note that the field inside the polymer is a superposition of the incoming and the reflected beam. Our choice of the angle of incidence $\phi = 34.05°$ ensures that for *p*-polarized beams the Fresnel reflection coefficient[23] vanishes. Thus, for *p* polarization [Eq. (2)], the field exciting the molecules is identical to the incoming field. For *s*-polarized field components [Eq. (3)] the reflection coefficient does not vanish. Thus a standing-wave pattern appears in the polymer film and in the cover slip with equal intensity fringes parallel to the interface. Thus, in principle, the excitation intensity seen by a molecule depends on its distance to the interface. However, for the chosen angle of incidence, ϕ, the fringe spacing is as large as 0.41λ. On the scale of the thickness of the polymer film (≈ 30 nm), the intensity can therefore be taken constant, $1.34(\pm 0.03)$ times larger than the incident field. This explains the appearance of the factor of 1.34^2 in Eq. (3).

The sign of one of the components of $\vec{\mathbf{d}}$ can be chosen at will because the dipole moment has no intrinsic directionality. We take the sign in Eq. (2) to be positive. The unknown sign in Eq. (3) is determined from the third exposure of the same molecule. The integrated count rate of single-molecule peaks in this exposure can be predicted from the previous images:

$$R_3 = \frac{E_3'^2}{2}|d_z' + 1.34 d_y'|^2. \tag{4}$$

The two possible choices of the sign in Eq. (3) result in two possible values of the predicted intensity. With the correct sign, Eq. (4) is satisfied when plugging in the measured value for R_3. This fully determines the projection of the dipole moment in the $y'-z'$ plane.

In order to determine the remaining out-of-plane component, two additional exposures (4), (5) from the second direction of incidence are required. The dipole component resulting from exposure (4) is given by

$$d_x'' = \pm[R_4/(1.34^2 E_4''^2)]^{1/2}. \tag{5}$$

The unknown sign of d_x'' can be determined from the fifth and all previous images. In analogy to Eq. (4), the predicted count rate for the last exposure reads

$$R_5 = \frac{E_5''^2}{2}|1.34 d_x'' + d_z''|^2. \tag{6}$$

The two tilted frames (prime and double prime) are related by a product of two rotation matrices by the angle $90° - \phi$ around the y and x axes. Therefore, the right-hand side of Eq. (6) can be expressed in terms of d_x'', d_y', and d_z'. Specifically, d_z'' and d_x' are given by

$$d_z'' = \cos\phi \sin\phi d_x' - \cos\phi d_y' + \sin^2\phi d_z',$$

$$d_x' = \frac{1}{\sin\phi}(d_x'' + \cos\phi d_z'). \tag{7}$$

With these relations d_z'' can be eliminated from Eq. (6) and the following condition can be derived to find the unknown sign in Eq. (5):

$$R_5 = \frac{E_5''^2}{2}|(1.34 + \cos\phi) d_x'' + d_z' - \cos\phi d_y'|^2. \tag{8}$$

Again, the two possible choices of the sign in Eq. (5) result in two possible values of the predicted intensity. With the correct sign, Eq. (8) is satisfied.

With these results, the components of $\vec{\mathbf{d}}$ in the laboratory frame can be calculated. The resulting orientation vector $\vec{\mathbf{d}}$ is parallel to the absorption dipole moment and its length is proportional to the absorption cross section of the molecule. Furthermore, the analytic expressions for the dipole components [Eqs. (2), (3), (5), and (7)] allow to calculate errors according to simple error propagation. We want to point out that recording further images from different directions of incidence adds redundant information that can improve the accuracy of the analysis. However, this is at the expense of a reduced time resolution.

III. RESULTS AND DISCUSSION

Figure 3 shows a typical series of five exposures of a molecule excited by the fields E_1', E_2', and E_3' from the first

Downloaded 27 May 2003 to 128.178.16.148. Redistribution subject to AIP license or copyright, see http://ojps.aip.org/jcpo/jcpcr.jsp

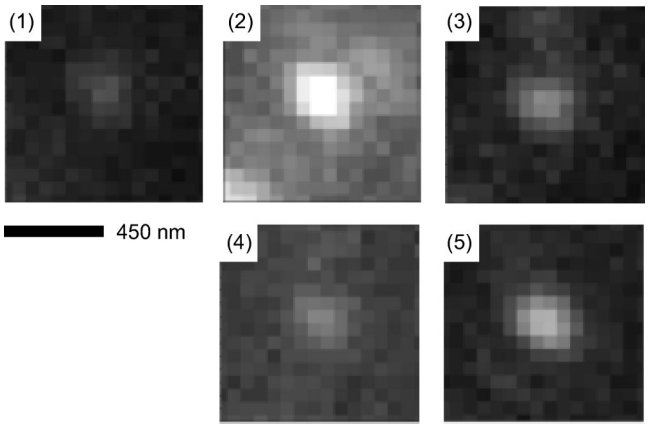

FIG. 3. Series of CCD images of a molecule for different polarizations and directions of incidence as indicated by the subscript numbers of the fields in Fig. 2. 1, 2, 3: first direction of incidence. 4, 5: second direction of incidence.

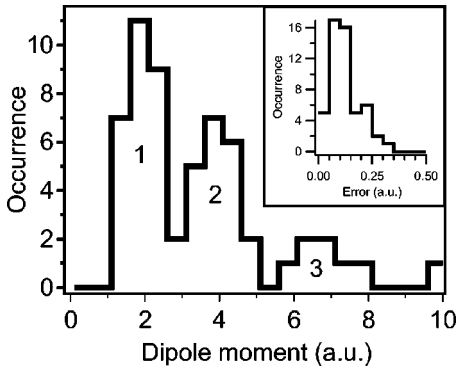

FIG. 4. Histogram of d values found from images 1, 2, and 4. The distribution shows three clear peaks assigned to single molecules, doubles, and triples. The inset shows the distribution of absolute errors obtained by error propagation from individual Gaussian fits.

direction of incidence [(1), (2), (3)] and by the fields E_4'' and E_5'' from the second direction of incidence [(4), (5)]. The polarization directions are indicated in Fig. 2. This series for a single molecule is taken from large images containing hundreds of molecules. The intensities of the fluorescence peak varies from bright to dim in accordance with a fixed orientation of the molecular absorption dipole during exposures. The total number of photons emitted by a molecule during the CCD exposure time is determined by fitting two-dimensional Gaussians with fixed width to the peaks using the Levenberg–Marquart algorithm implemented in IGOR PRO (data-analysis software, Wavemetrics, Lake Oswego, Oregon). The initial values for the peak positions are found using the sum of images 1, 2, and 4 by applying an algorithm which neglects very weak peaks. The algorithm also employs a finite grid width which is slightly larger than the apparent spatial resolution. It is thus not possible to discriminate between peaks that are too close. Such multiple peaks are fitted by a single Gaussian with increased intensity. Fitting also yields the local background at the position of a peak which is proportional to the squared electric excitation field (after subtraction of dark counts, data not shown). The background in the image may vary because of the Gaussian intensity profile of the incident beams and also because of interference between the incoming and reflected beam. Accordingly, in the images with s polarization the background is larger by a factor of 1.34^2 as compared to the p-polarized excitation. The fitting procedure further provides an estimate for the standard deviation of the fit parameters. We found average relative errors of 2% and 10% of the background and the integrated intensity, respectively. They were used to compute the errors for the components of the emission dipole by error propagation. A finite angle between the transition dipole moments for absorption and emission does not affect the analysis and interpretation of the data, although different emission dipole orientations result in different collection efficiencies. This is because an orientation-dependent pattern is emitted and only a finite solid angle is collected. However, this effect has no influence on the data since for each individual molecule the collection efficiency is constant for all of the five exposures.

Once the Cartesian components of the dipole moment $\vec{\mathbf{d}}$ are known they can be transformed into spherical coordinates, d, φ, and ϑ, which are directly related to orientations. Here d is proportional to the absorption cross section, φ is the azimuth angle counted from the positive x axis and running from $-180°$ to $+180°$, and ϑ the out-of-plane angle counted from the $x-y$ plane (see Fig. 2).

Using only the images 1, 2, and 4 the absolute value of the dipole vector $\vec{\mathbf{d}}$ can be extracted. A histogram of 60 absolute values $|d|$ is shown in Fig. 4. Arbitrary units are used for d (i) because here we are only interested in relative magnitudes and (ii) because reliable numbers for the collection efficiency and for the fluorescence quantum yield are difficult to obtain. Nevertheless, we can estimate the most frequent absorption cross section to be about 10^{-16} cm^2, which is typical for the dye used. The histogram clearly shows three peaks that we attribute to single molecules, pairs of molecules, and triples of molecules. As discussed above the occurrence of pairs and triples is caused by (i) the fitting and peak finding routine that has a certain grid width and (ii) the limited spatial resolution of the optical microscope. In clusters, DiI molecules are treated as individuals since antibunching experiments on clusters show that DiI does not aggregate at these concentrations.[24] Therefore, individual dipole moments add up, finally leading to the observed multiple-peaked distribution. In the further analysis we only used spots that were contained in the first, the single-molecule peak. We further excluded molecules from the analysis that exhibit a relative error of the length of the dipole vector $\Delta d/d$ larger than 20%. The error is calculated by error propagation using the errors obtained from the Gaussian fit. Large errors can occur as a result of time-dependent dynamical behavior in the fluorescence of single molecules. At this point it should be emphasized that the ability to select only molecules with the desired behavior for further analysis is unique to single-molecule experiments and strongly improves the accuracy and reliability of the results.

The actual assignment of orientations is done using Eqs.

Downloaded 27 May 2003 to 128.178.16.148. Redistribution subject to AIP license or copyright, see http://ojps.aip.org/jcpo/jcpcr.jsp

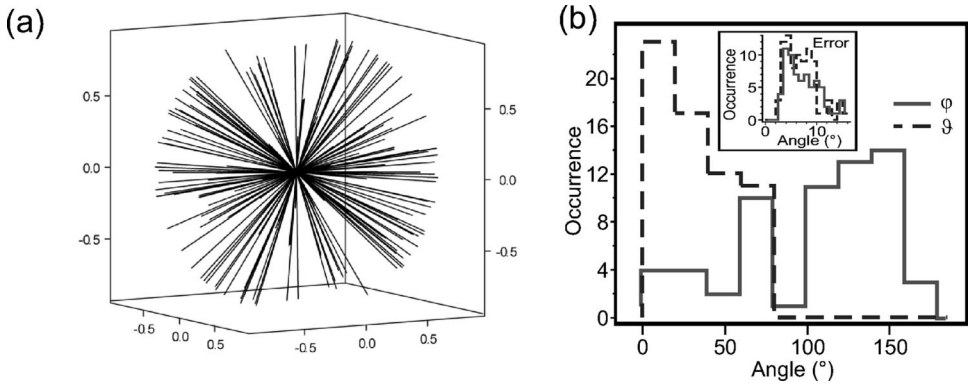

FIG. 5. Distribution of single-molecule orientations in a spin-coated polymer film. (a) Orientational representation: the lines indicate the orientations of normalized dipole orientation vectors. (b) Histograms of dipole orientation angles (solid line for ϕ and dashed line for ϑ). The inset in (b) shows the distribution of errors for the angles ϕ and ϑ obtained by error propagation from individual Gaussian fits.

(4) and (6). Since the data are not free of noise, we assume the correct sign of d_y' and d_x'' to be the one that best satisfies Eqs. (4) and (6), respectively. If molecules bleach during the experiment or show strong intensity fluctuations on a relevant time scale, these equations may be violated significantly for both signs. We therefore discard those molecules for which the left-hand side of Eqs. (4) or (6) is not within the 95% confidence interval of the right-hand side for either sign chosen. After applying these selection criteria, 90 molecules were used to compute the distribution of orientations.

We studied the effect of shot noise in the data on the result of our analysis using computer simulations. When assuming a noise level similar to that present in our experimental data we obtained a value of 12% of the width of the distribution of $|d|$ divided by the peak position (i.e., the relative width), much smaller than the first peak in Fig. 4. However, this small width is in good agreement with the width of the distribution of errors obtained by error propagation from individual Gaussian fits. We attribute the increased width in the distribution of the measured data as compared to the simulation to two additional sources of noise: (i) dynamic variations of the local environment of the fluorophores and (ii) fluctuating fluorescence emission (blinking) or absorption (wobbling, flipping). The simulation also showed that for a small number of molecules ($<6\%$), having exceptionally large intensity errors, the test equations (4) and (6) yield wrong signs for the Cartesian components and therefore wrong orientations are assigned.

Using the spherical angles ϑ and φ, the distribution of orientations is visualized in Fig. 5(a) by lines drawn through the origin. The distribution is found to be compatible with an isotropic distribution as expected for chromophores embedded in a polymer film. Histograms of the orientation angles are shown in Fig. 5(b). The distribution of ϑ decays towards 90°, again consistent with an isotropic distribution of molecular orientations. Macklin *et al.*[20] observed a similar distribution of ϑ for a smaller number of molecules using an independent approach. There are some residual variations in the distribution of the angle φ, which are due to the limited number of molecules rather than due to a true anisotropy.

Again computer simulation were used to exclude possible artifacts introduced by the analysis. When starting with an isotropic distribution of dipole orientations, after adding noise, the algorithm outlined above recovers the identical isotropic set of orientations. We found that the standard deviation of the orientational error is smaller than 2° for all angles.

To summarize all the information obtained from a 3D-OPTO image series we show the orientation and the position of 20 randomly selected DiI molecules in a 3D representation in Fig. 6. The double arrows symbolize the orientation of molecules at their position within the sample plane.

Ideally, systems that are to be investigated with the present method should exhibit slow orientation motion on the timescale necessary to acquire at least five images ($\approx$ down to 5 ms). This condition can be relaxed if some components of orientational diffusion are very fast (e.g., wobbling in a cone) and can be averaged out. As is typical for single-molecule experiments, each set of exposures provides a whole distribution of orientations. Thus it should be possible to measure time-averaged orientations in semi-ordered systems like membranes and liquid crystals with good accuracy.

IV. CONCLUSIONS

In conclusion we have described and demonstrated a method of single-molecule microscopy, 3D-OPTO, that enables direct observation of both three-dimensional orientation and position of single fluorophores within the sample plane. This is accomplished by illumination from different

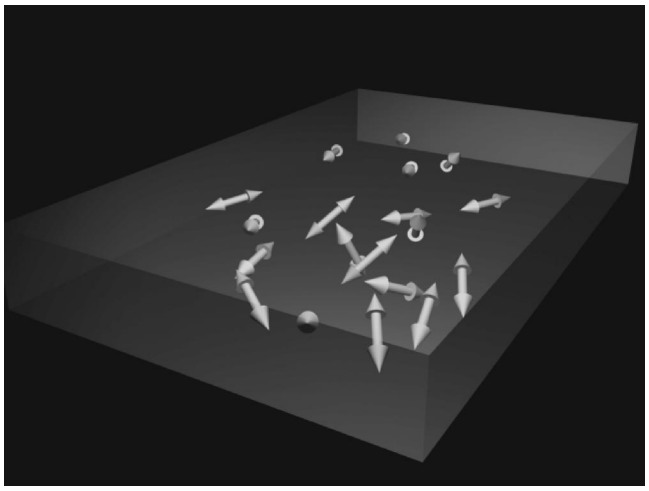

FIG. 6. 3D representation of the full information (orientation and position) obtained in the experiment. Image area 9 μm$\times$15μm.

Downloaded 27 May 2003 to 128.178.16.148. Redistribution subject to AIP license or copyright, see http://ojps.aip.org/jcpo/jcpcr.jsp

directions of incidence with linearly polarized beams. The full signal-to-background ratio and the full diffraction-limited resolution can be exploited because defocusing and the use of aberrations are not necessary. Using wide-field microscopy, large numbers of molecules can be investigated in parallel with very low background. The method is inexpensive and compatible with standard fluorescence microscopy equipment. Knowing the three-dimensional orientation of fluorophores, especially in combination with other techniques, 3D-OPTO enables the selective excitation of subensembles. Distance measurements using single-pair FRET can be greatly improved if the true orientation of the fluorophores is known. 3D-OPTO has considerable potential for studying translational and rotational motion of single molecules on a 100 ms time scale. This is of particular interest in the study of dynamical processes for example in lipid membranes and motor proteins.

ACKNOWLEDGMENTS

The authors are grateful to T. Latychevskaia, A. Renn, and J.-M. Segura for continual support. This project has been funded by the ETH Zürich.

[1] *Single-Molecule Optical Detection, Imaging and Spectroscopy*, edited by T. Basché, W. E. Moerner, M. Orrit, and U. P. Wild (VCH, Weinheim, 1997).
[2] *Frontiers in Chemistry: Single Molecules* [Science **283,** 1670 (1999)].
[3] Th. Schmidt, G. J. Schütz, W. Baumgartner, H. J. Gruber, and H. Schindler, Proc. Natl. Acad. Sci. U.S.A. **93**, 2926 (1996).
[4] G. J. Schütz, G. Kada, V. P. Pastushenko, and H. Schindler, EMBO J. **19**, 892 (2000).
[5] K. Adachi, R. Yasuda, H. Noji, H. Itoh, Y. Harada, M. Yoshida, and K. Kinosita , Jr., Proc. Natl. Acad. Sci. U.S.A. **97**, 7243 (2000).
[6] K. Kitamura, M. Tokunaga, A. H. Iwane, and T. Yanagida, Nature (London) **397**, 129 (1999).
[7] Y. Sako, S. Minoghchi, and T. Yanagida, Nat. Cell Biol. **2**, 168 (2000).
[8] H. P. Lu, L. Xun, and X. S. Xie, Science **282**, 1877 (1998).
[9] L. Edman and R. Rigler, Proc. Natl. Acad. Sci. U.S.A. **97**, 8266 (2000).
[10] T. J. Ha, A. Y. Ting, J. Liang, W. B. Caldwell, A. A. Deniz, D. S. Chemla, P. G. Schultz, and S. Weiss, Proc. Natl. Acad. Sci. U.S.A. **96**, 893 (1999).
[11] X. Zhuang, L. E. Bartley, H. P. Babcock, R. Russell, T. J. Ha, D. Herschlag, and S. Chu, Science **288**, 2048 (2000).
[12] F. Oesterhelt, D. Oesterhelt, M. Pfeiffer, A. Engel, H. E. Gaub, and D. J. Muller, Science **288**, 143 (2000).
[13] S. Weiss, Science **283**, 1676 (1999).
[14] T. J. Ha, Th. Enderle, D. F. Ogletree, D. S. Chemla, P. R. Selvin, and S. Weiss, Proc. Natl. Acad. Sci. U.S.A. **93**, 6264 (1996).
[15] I. Sase, H. Miyate, S. Ishiwata, and K. Kinosita, Proc. Natl. Acad. Sci. U.S.A. **94**, 5646 (1997).
[16] T. J. Ha, T. A. Laurence, D. S. Chemla, and S. Weiss, J. Phys. Chem. **103**, 6839 (1999).
[17] J. Sepiol, J. Jasny, J. Keller, and U. P. Wild, Chem. Phys. Lett. **273**, 444 (1997).
[18] R. M. Dickson, D. J. Norris, and W. E. Moerner, Phys. Rev. Lett. **81**, 5322 (1998).
[19] A. P. Bartko and R. M. Dickson, J. Phys. Chem. B **103**, 3053 (1999); **103**, 11237 (1999).
[20] J. J. Macklin, J. K. Trautman, T. D. Harris, and L. E. Brus, Science **272**, 255 (1996).
[21] B. Sick, B. Hecht, and L. Novotny, Phys. Rev. Lett. **85**, 4482 (2000).
[22] D. Axelrod, in *Light Microscopy in Biology—A Practical Approach*, 2nd ed., edited by A. J. Lacey (Oxford University Press, Oxford, 1997).
[23] M. Born and E. Wolf, *Principles of Optics*, 6th ed. (Cambridge University Press, Cambridge, UK, 1980).
[24] C. G. Hübner (private communication).

Downloaded 27 May 2003 to 128.178.16.148. Redistribution subject to AIP license or copyright, see http://ojps.aip.org/jcpo/jcpcr.jsp